ELSEVIER

Journal of Photochemistry and Photobiology A: Chemistry 130 (2000) 145–156

Journal of Photochemistry and Photobiology A:Chemistry

www.elsevier.nl/locate/jphotochem

(Photo)electrochemical behavior of selected organic compounds on TiO_2 electrodes. Overall relevance to heterogeneous photocatalysis

A. Taghizadeh [a], M.F. Lawrence[a,1], L. Miller [b], M.A. Anderson [b], N. Serpone [a,*]

[a] *Department of Chemistry and Biochemistry, Concordia University, 1455 de Maisonneuve Blvd. West, Montreal, QC, Canada H3G 1M8*

[b] *Water Science and Engineering Laboratory, Department of Civil and Environmental Engineering, University of Wisconsin, 660 North Park Street, Madison, WI 53706-1484, USA*

Received 26 April 1999; received in revised form 7 September 1999; accepted 13 September 1999

Abstract

Oxidation potentials of resorcinol, 4-chlororesorcinol, 4,6-dichlororesorcinol, catechol, 3,4-dihydroxybenzoic acid and 1,2,4-trihydroxybenzene were measured on particulate TiO_2 (Degussa P-25) thin films, immobilized on optically transparent SnO_2 conducting glass electrodes, by cyclic voltammetry in 0.5M KCl aqueous electrolyte solutions. The effect of adsorption on oxidation potentials was examined with the compounds adsorbed on the TiO_2 particle surface. Scan rate dependencies of oxidation peak currents indicate that adsorbed species are consistently characterized by less positive oxidation potentials compared to those attributed to solution free species; the difference ranges from about 0.2 to 0.8 V. Results show that depending on the nature of the working electrode, associating a single oxidation potential to such compounds does not adequately describe their electrochemical behavior. Such observations have relevance in heterogeneous photocatalysis in that predictions of whether a substance will be photooxidized or photoreduced cannot be based on Fermi levels (redox potentials) of the redox couples in homogeneous solutions.

Keywords: Photoelectrochemical behavior; Oxidation potentials; Titaria electrodes; Cyclic voltammetry; Photocatalysis; Adsorption effects

1. Introduction

Water contamination in the last few decades from extended agricultural and industrial processes has led to growing concerns on the quality of water [1]. As a result, decontamination of natural and drinking water has become an increasingly important task in environmental protection [2]. Detoxification of water has typically relied on conventional strong oxidative methods (e.g. chlorination and ozonation) which tend to be hazardous and thus of an undesirable nature [3]. Non-destructive technologies in current use (e.g. air-stripping and carbon adsorption) also present certain disadvantages. For example, air-stripping used to remove volatile contaminants converts a liquid contamination problem into an air pollution problem; carbon adsorption produces a hazardous solid which ultimately is disposed either by combustion or, as is more often the case, by burial [3].

Limitations associated with these traditional methods have resulted in developments of new techniques whose end-products are non-toxic. An interesting process that has gained popularity in recent years is the photocatalyzed mineralization of organic pollutants by irradiated semiconductor photocatalysts [4–25]. One of the methods relies on photoelectrochemical processes, whereby redox reactions are initiated by absorption of a photon by the photocatalyst which is immobilized on an optically transparent electrode (OTE) forming an interface with the electrolyte [26]. The popularity of this method has arisen from the fact that the mineralized product it produces is harmless to the environment. The semiconductor that has attracted most attention for this purpose is titania, TiO_2, mostly in the anatase form [4–20]. The prevalent use of TiO_2 is attributed to its abundance and relatively low cost, to its relative insolubility under most conditions, to its photochemical stability and to its non-toxic nature [19].

Photochemical reactions on semiconductors can be separated into two groups: (i) semiconductor-mediated photocatalysis in which hydroxyl radicals, $^{\bullet}OH$, generated from the oxidation of chemisorbed hydroxide ions and/or water by the valence band holes at the surface of TiO_2 particles,

* Corresponding author. Tel.: +1-514-848-3374; fax: +1-514-848-2868.
E-mail addresses: lawrence@vax2.concordia.ca (M.F. Lawrence), serpone@vax2.concordia.ca (N. Serpone).
[1] Co-corresponding author.

1010-6030/00/$ – see front matter
PII: S1010-6030(99)00194-X

react with pre-adsorbed organic compounds at the particle/solution interface; and (ii) by direct oxidative transformation of the compounds that need to diffuse from the bulk solution to the semiconductor particle surface [27,28]. Both these views have been the object of lively and substantive debates in the literature.

Numerous publications on heterogeneous photocatalysis have reported several aspects of water remediation initiated by irradiation of the TiO_2 photocatalyst [1–26]. In most cases, if not all, adsorption of the polluting compounds under examination appears to play an important role in the degradation process [19]. In all the photochemical and photoelectrochemical processes, a single redox potential which reflects the oxidation potential of dissolved species in bulk solution has been used to describe the redox behavior of the organic compound, regardless of its actual state (free or adsorbed on the TiO_2 surface) [5,7,8,26]. Indeed, predictions of whether a given pollutant metallic ion, M^{n+}, or a pollutant organic compound, R, that can be reduced or oxidized, respectively, by illuminated titania particles has always relied on comparison of the Fermi levels of the $M^{n+}/M^{(n-1)+}$ and R/R^+ redox couples in homogeneous solutions (often nonaqueous media for the organics) relative to the appropriate conduction and valence flat band potentials of the photocatalyst.

The aim of this study was to assess the redox potentials of selected aromatic compounds as free species in solution and as adsorbates on the TiO_2 electrodes and to show that the redox potentials of adsorbed organic compounds differ significantly from those of non-adsorbed compounds for which (photo)electrochemical oxidation is diffusion-controlled.

2. Experimental

2.1. Electrode preparation

Optically transparent conducting glass plates (SnO_2, Pittsburgh Plated Glass, $50\,\Omega\,cm^{-1}$; 2 cm × 3 cm) were cleaned in a sulfochromic acid solution (12 ml of a saturated aqueous solution of chromium trioxide in 2.7 l of H_2SO_4) for ca. 5 min and then rinsed several times with water followed by a further rinse (three times) with distilled/deionized water. The plates were subsequently dried under a stream of nitrogen gas prior to utilization. Three different types of TiO_2 electrodes were prepared using these conducting glass plates.

2.1.1. Particulate TiO_2 electrodes

A dispersion of TiO_2 particles was prepared by suspending a known quantity of Degussa P-25 titania in water ($10\,g\,l^{-1}$) to which 0.5 ml of concentrated HCl was added and then stirred for ca. 4 h. Subsequently, 0.4 ml of the TiO_2 slurry (cooled to 0°C in an ice bath) was applied over a 2 cm × 2 cm surface area of the conducting glass plate. After drying overnight, the TiO_2-coated electrodes were sintered at 450°C under ambient atmosphere for 1 h. The thickness of the TiO_2 films obtained by scanning electron microscopy (SEM) of the film's cross section was $22 \pm 5\,\mu m$. The upper two panels in the micrographs of Fig. 1 show the top view of a TiO_2 film on the conducting glass plate at two magnification factors; the lower two panels show side views of the same electrode.

2.1.2. Preparation of glassy TiO_2 electrodes

An aqueous sol of TiO_2 was prepared by combining water, $Ti^{IV}(i\text{-}PrO)_4$, and 70% HNO_3 at a ratio of 800/66/5.7 ml, respectively. The mixture was stirred for 3 days to obtain a clear suspension, subsequent to which it was dialyzed in 3500 MW-cutoff dialysis tubing for 3 days. The dialyzing water was changed daily and the final pH of the sol was 3.5. Conducting glass plates were dipped into the sol until all but ~5 mm were submerged. The specimens were withdrawn at $2.6\,cm\,min^{-1}$ and allowed to dry in ambient air. The coated samples were fired at 300°C for 1 h. Profilometry tests on quartz plates coated under otherwise identical conditions show the thickness of the coatings to be 110 ± 10 nm.

2.1.3. Preparation of tandem TiO_2 electrodes

The glassy TiO_2 electrodes described in Section 2.1.2 were also coated with a particulate TiO_2 (P-25) film as described in Section 2.1.1.

2.2. Instrumentation

The three-electrode cell specifically designed for these experiments (Fig. 2) was made of pyrex glass, fitted with a quartz glass window to allow for photoelectrochemical experiments. The area of the working electrode in contact with the solution was $0.4\,cm^2$. The counter electrode was a $0.5\,cm^2$ platinum foil; the reference electrode was a saturated calomel electrode (SCE). The light source was a Bausch & Lomb 150 W Xenon lamp.

Cyclic voltammograms were obtained with a BAS-100A electrochemical analyzer (Bioanalytical Systems). Current-voltage responses were recorded on a DMP-40 series digital plotter (Ametek/Houston Instruments).

2.3. Methods

The model compounds used in this study are illustrated in Fig. 3. Set A consists of resorcinol (RSRCL; Fisher Scientific, 99%), 4-chlororesorcinol (4-CR; Aldrich, 98%) and 4,6-dichlororesorcinol (4,6-DCR; Aldrich, 97%). Set B consists of catechol (CC; Anachemia, 99+%), 3,4-dihydroxybenzoic acid (3,4-DHBA; Acros Organics, 97%) and 1,2,4-trihydroxybenzene (1,2,4-THB; Aldrich, 99%). All compounds were used as received without further purification.

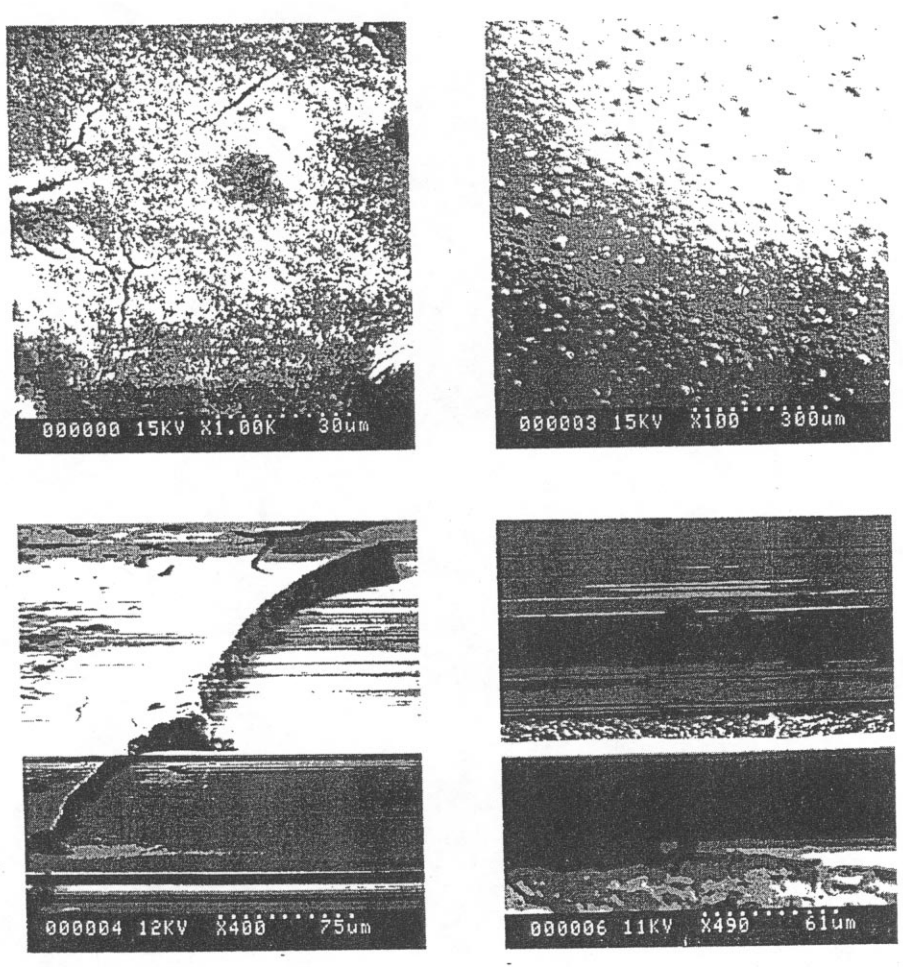

Fig. 1. Scanning electron micrograph of particulate TiO_2 electrode: top view of the thin film electrode are shown in the two upper panels; the lower two panels illustrate two different side views.

Unless noted otherwise, oxidation potentials were determined at an optimal concentration of 0.005M in aqueous 0.5M KCl electrolyte solutions. All solutions were prepared with distilled/deionized water. A 15 ml sample of the 0.005M solution was placed in the cell and then purged with nitrogen gas (99.998%) for ca. 15 min prior to each run. Compounds treated this way are referred to as dissolved species. Experiments carried out in acetonitrile (Sigma-Aldrich, HPLC grade) used tetrabutylammonium hexafluorophosphate (TBAHFP, Aldrich) as the supporting electrolyte also at a concentration of 0.5M.

Determination of oxidation potentials of species under imposed adsorption conditions was carried out on TiO_2 electrodes in which the compounds were first dissolved in methanol to give 0.1M solutions. Two consecutive 10 μl portions of the 0.1M solution were applied to the TiO_2 electrode, following which it was air-dried for several minutes and then attached to the cell. A 15 ml aqueous solution containing the 0.5M KCl supporting electrolyte (pre-purged with nitrogen) was added prior to the execution of each run. Compounds treated in this manner are referred to as adsorbed species.

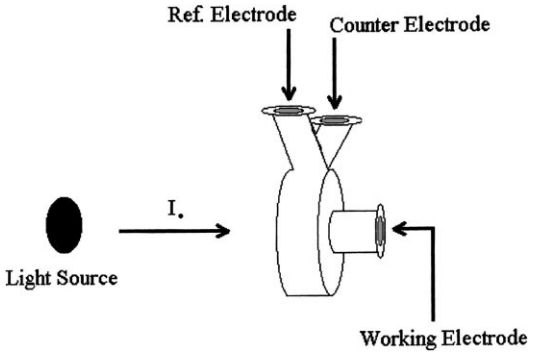

Fig. 2. Electrochemical cell used in the cyclic voltammetric measurements.

Single cycle runs were performed at scan rates of 25, 50, 100, 150 and 200 $mV\,s^{-1}$. Every run was recorded using a fresh electrode and was taken initially from negative to positive potentials. Each of the reported values for oxidation

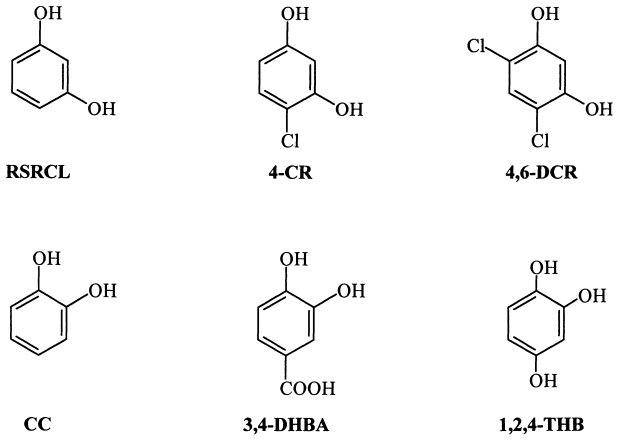

Fig. 3. Structures of the aromatic substances examined in this study. Set A compounds are shown in the three upper structures of the first row, whereas set B compounds are in the second row.

potentials and peak currents represents an average of at least five separate runs. Unless otherwise noted, all oxidation potentials are given versus the SCE reference electrode. Solutions were freshly prepared daily. Experiments were carried out at ambient temperature.

3. Results and discussion

The working potential ranges of the electrodes were first determined by running cyclic voltammograms on the 0.5M KCl supporting electrolyte only. They were −0.30 to 1.70 V for the particulate and tandem TiO_2 electrodes, and 0.30 to 1.70 V for the glassy TiO_2 electrode. The working potential window for the particulate TiO_2 electrodes in acetonitrile containing 0.5M of the supporting electrolyte TBAHFP was −0.30 to 2.80 V. No oxidation peaks were observed in these potential ranges when the sample consisted of the supporting electrolyte only, regardless of whether the voltammogram was taken in the dark or under illumination.

Figs. 4a–c compares the voltammograms obtained for the oxidation of 4-CR in 0.5M KCl on glassy TiO_2, tandem TiO_2 and particulate TiO_2 electrodes, respectively. The oxidation potential of 4-CR, taken at the maxima of the anodic peak current, appears at ca. 1.3 V for the tandem and particulate TiO_2 electrodes and at ca. 1.5 V for the glassy TiO_2 electrode. The voltammogram in Fig. 4a indicates that the working potential window for the glassy TiO_2 electrode is diminished by ca. 0.6 V on the negative potential side, relative to the potentials of the particulate and tandem TiO_2 electrodes which are essentially the same. These results demonstrate that oxidation of 4-CR occurs at the surface of the TiO_2 film at both the tandem and the particulate TiO_2 electrodes, and that no compound penetrates through the TiO_2 thin film to be oxidized at the underlying SnO_2 OTE. {Note that although Sn may diffuse through the TiO_2 film as suggested by one reviewer, it is highly unlikely for it to reach the surface of the TiO_2 deposit, under our conditions, where most of the oxidation takes place}. Henceforth, measurements were performed on the particulate TiO_2 electrodes only.

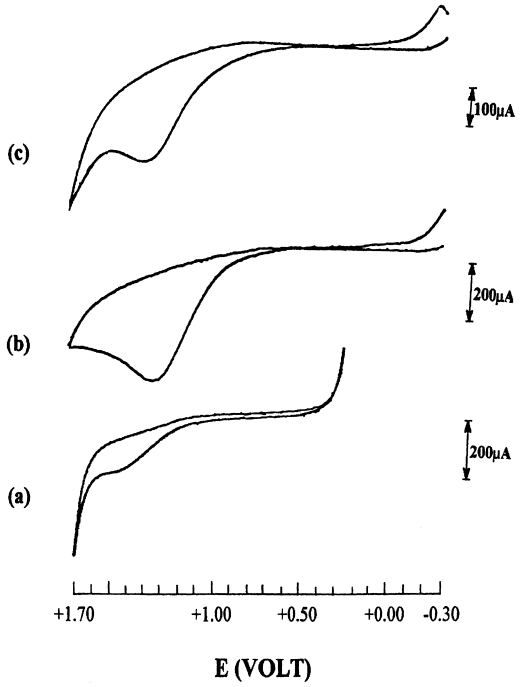

Fig. 4. Cyclic voltammograms of 4-chlororesorcinol, 4-CR, in a 0.5M KCl electrolyte solution on (a) a glassy TiO_2 electrode, (b) a tandem TiO_2 electrode, and (c) a particulate TiO_2 electrode.

The model organic compounds used to study the effects of adsorption on the oxidation potentials are grouped into two sets (Fig. 3). The first set A consists of resorcinol (RSRCL), 4-chlororesorcinol (4-CR) and 4,6-dichlororesorcinol (4,6-DCR) in which the hydroxyl groups on the benzene ring are at the meta position. The second set of compounds, set B, consists of catechol (CC), 3,4-dihydroxybenzoic acid (3,4-DHBA) and 1,2,4-trihydroxybenzene (1,2,4-THB) in which hydroxyl groups are in the ortho position. The stereochemical configuration of the latter three compounds should favor chemisorption on the TiO_2 surface by formation of surface chelate complexes with the surface Ti^{IV} ions [29].

Cyclic voltammetry of a diffusion-controlled redox process conforms to the Randles-Sevcik equation given at ambient temperature as [30,31],

$$I_p = 2.69 \times 10^5 n^{3/2} A C_o D^{1/2} \nu^{1/2} \quad (1)$$

where I_p is the oxidation peak current, n the number of electrons involved in the oxidation, A the surface area of the electrode in contact with the solution, C_o the bulk concentration of the analyte, D the diffusion coefficient, and ν is the scan rate. Eq. (1) suggests that a plot of I_p versus $\nu^{1/2}$ for a diffusion-controlled process should be linear and have a zero-intercept. Deviations from this behavior are expected if the redox process involves adsorbed species. Another anticipated effect when redox processes involve adsorbed species is the appearance of additional peaks in the cyclic voltammogram which may, depending on the free energy of

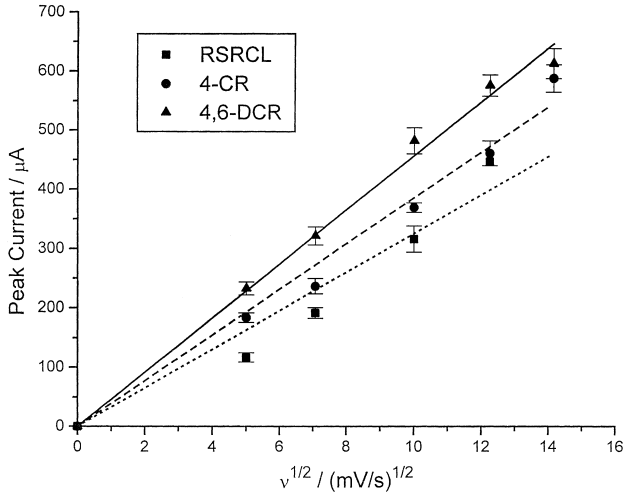

Fig. 5. Oxidation peak current vs. the square root of the scan rate for resorcinol, 4-chlororesorcinol, and 4,6-dichlororesorcinol in aqueous 0.5M KCl media for diffusion-controlled processes (see Eq. (1) in text).

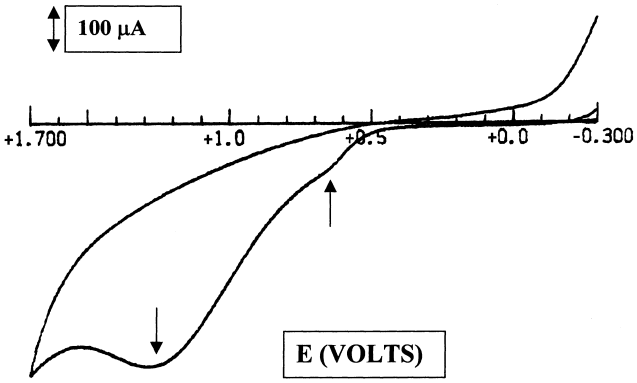

Fig. 6. Cyclic voltammogram of 4-chlororesorcinol in aqueous 0.5M KCl on a dark particulate TiO_2 electrode (see text).

adsorption, either precede (pre-peak) or follow (post-peak) the peak attributed to the diffusion-controlled process [31].

4. Compounds of set (A)

4.1. Dissolved species

The electrochemical behavior of RSRCL, 4-CR, and 4,6-DCR, was assessed after dissolution of these species in an unbuffered electrolyte solution. The pH ranged from 5.8 to 6.0. As exemplified in Fig. 4 for 4-CR, all three compounds exhibited a single oxidation peak on particulate TiO_2 electrodes. At a scan rate of 100 mV s^{-1}, oxidation potentials were 1.33 ± 0.01 V (RSRCL), 1.36 ± 0.04 V (4-CR) and 1.43 ± 0.01 V (4,6-DCR). In all cases, I_p scales linearly with $\nu^{1/2}$ with near zero intercept (Fig. 5), in accord with the Randles-Sevcik Eq. (1) for a diffusion-controlled process.

4.2. Adsorbed species

Experiments conducted with RSRCL, 4-CR and 4,6-DCR under imposed adsorption conditions on particulate TiO_2 electrodes showed that the voltammogram for RSRCL remained unchanged relative to the voltammogram under diffusion-controlled conditions.[2] By contrast, two oxidation peaks were observed for adsorbed 4-CR (Fig. 6) and 4,6-DCR. The peak around 1.3 V for both 4-CR (Fig. 4c) and 4,6-DCR (dissolved species) was still present with an additional peak appearing at ca. 0.6–0.7 V at pH 6 (4-CR and 4,6-DCR; Table 2). The additional oxidation peaks were seen only when the compounds existed as adsorbates, and therefore strongly suggest that they originate from initially adsorbed reactants. Moreover, the magnitude of the peak currents compared to peak currents obtained for free compounds, together with the unusual behavior of these peaks with respect to the Randles-Sevcik Eq. (1) (peak current dependency on the square root of scan rate), provides additional support for this conclusion. Thus, the adsorbed 4-CR displays an oxidation potential at ca. 0.6 V less positive than 4-CR in solution, which no doubt is due to the effect of surface interactions with the substrate.

The nature of RSRCL, 4-CR and 4,6-DCR does not provide conditions for chemisorption as surface chelate complexes. In these cases, adsorption is typically due to weak Van Der Waals interactions of the molecules with the surface of the TiO_2 electrodes [32–34]. Electronegative ring substituents such as chlorine and oxygen on the benzene ring impart a dipole moment to these species which leads to weak adsorption interactions between the compounds and the electrode surface [34]. The polarity created by the electronegative oxygens on RSRCL is likely offset by the hydrogens together with the resonance effect of the benzene ring [32,33]. This negates a strong polarity and leads to very weak adsorption of RSRCL on TiO_2, consistent with the absence of an oxidation pre-peak for resorcinol. By contrast, 4-CR and 4,6-DCR contain chlorine in addition to oxygen which strongly affects the charge density distribution, thereby creating a net dipole moment on these compounds [34,35]. The stronger adsorption of the polar molecules on the TiO_2 electrode surface leads to the observed oxidation pre-peak.

The peak current dependency on the square root of the scan rate (Fig. 7) was used to further analyze the electrochemical behavior of these compounds on TiO_2 electrodes. The surface area of the electrode exposed to the solution should limit the amount of adsorbate [20,31]. In the present study, a large concentration of organic compound was initially deposited on the surface of the electrode. On addition of the electrolyte, some of the excess material may have diffused from the electrode surface to the solution which manifested itself as a diffusion-controlled oxidation peak, and gave rise to two oxidation peaks. Recall that the presence of

[2] Observation of one peak for resorcinol under dissolved and adsorbed conditions precludes any residual methanol adsorbed on the TiO_2 deposit that might be oxidized photoelectrochemically.

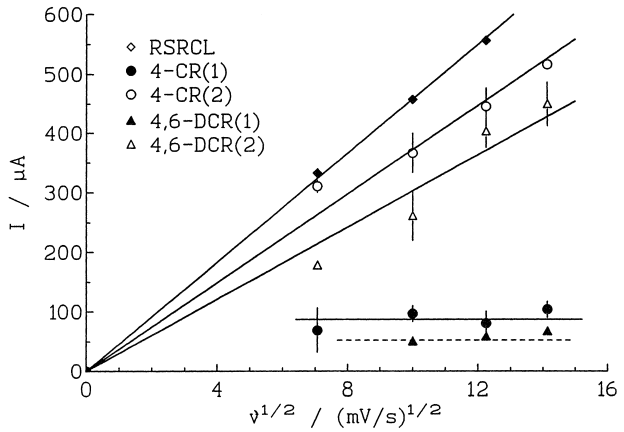

Fig. 7. Oxidation peak current vs. the square root of the scan rate (Eq. (1); see text) for resorcinol, 4-chlororesorcinol and 4,6-dichlororesorcinol under imposed adsorption conditions.

adsorbed species on the electrode surface was an imposed condition. Consequently, the amount of adsorbed species on the electrode surface varied with time because of desorption. The oxidation peak due to adsorption showed little or no increase in peak current on increasing the scan rate (Table 2), whereas the peak due to diffusion scales linearly with $\nu^{1/2}$ (peaks at most positive potentials for 4-CR and 4,6-DCR).

4.3. Effect of illumination

Oxidation of the set A model compounds on TiO_2 electrodes was also examined under illumination to explore the effect of light absorption by the semiconductor on the redox potentials and on the peak currents. Fig. 8 illustrates the voltammogram of 4-CR at a scan rate of $100\,mV\,s^{-1}$ and at pH 6. The anodic baseline shift of ca. $100\,\mu A$ seen on the oxidation of these compounds on illuminated TiO_2 is in keeping with the photoactivity of the semiconductor [36].

Contrary to expectations whereby redox potentials shift under illumination [37], the oxidation potentials of RSRCL, 4-CR, and 4,6-DCR on illuminated TiO_2 electrodes showed no significant changes relative to those obtained under dark conditions (see Table 1). The lack of any significant shift may be the result of the low light irradiance employed to illuminate the electrodes (ca. $30\,mW\,cm^{-2}$), or to the inability of the organic substances examined to interact with

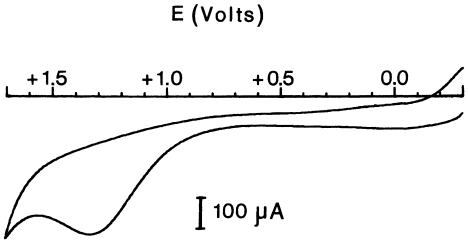

Fig. 8. Cyclic voltammogram of 4-chlororesorcinol in aqueous 0.5M KCl media on an illuminated particulate TiO_2 electrode at pH 6; scan rate $100\,mV\,s^{-1}$.

the photogenerated minority carriers at the electrode surface [37–39]. By contrast, illumination does change oxidation peak currents of set A model compounds. The difference between peak photocurrents and peak dark currents ($I_i - I_d$) decreases with increase in the number of chlorine substituents on the resorcinol moiety as depicted in Fig. 9 as ($I_i - I_d$) versus scan rate ν. Photooxidation efficiency of the illuminated TiO_2 electrode appears to decrease with an increase in the number of such electronegative substituents on the phenyl ring.

4.4. Effect of pH

4-chlororesorcinol was chosen to examine the pH effect (pH 6 and 3) on oxidation potentials and peak currents since the oxidation peaks were well resolved under various pH conditions, yielding precise measurements of E and I_p. Oxidation potentials were not affected when the working electrode was platinum. An overall increase in peak currents was observed in more acidic media (pH 3, Table 1) consistent with the overall pH sensitive nature of redox reactions of phenols and quinones [40]. Under dark conditions, the oxidation potentials showed only slight increases from pH 6 to 3; peak currents generally increased at the lower pH albeit not monotonically at the various scan rates.

The band positions for a metal-oxide semiconductor electrode, E_{CB} and E_{VB}, are pH-dependent [41,42], with E_{CB} being given by Eq. (2) [41]:

$$E_{CB}(V) = -0.5 - 0.06(pH) \quad (2)$$

where $-0.5\,V$ represents the E_{CB} redox position (versus SCE) of the TiO_2 electrode at pH 0. Consequently, a shift of ca. $0.18\,V$ to more positive potentials is expected at pH 3 relative to pH 6 for both the conduction band and for the species being oxidized on the TiO_2 electrodes. At a scan rate of $100\,mV\,s^{-1}$, the increase in oxidation potentials for 4-CR from pH 6 to 3 is in the range 0.04–0.15 V for dissolved species under dark and illuminated conditions (see Table 1) and 0.11–0.13 V for adsorbed species under dark conditions (see E_1 in Table 2). Any deviations from expectations has been alluded to the presence of surface defects (i.e. surface states) on TiO_2 electrodes [43], and to changes in adsorption owing to the positively charged surface at pH 3 versus the neutral TiO_2, surface at pH 6, i.e. at the point of zero charge for titania [44]. Thus, the dipolar model compounds should interact adsorptively to a greater extent with the positively charged surface at pH 3.

5. Compounds of set (B)

5.1. Dissolved species

The electrochemical behavior of the model compounds CC, 3,4-DHBA and 1,2,4-THB was first examined on a plat-

Table 1
Redox potentials (vs. SCE) and peak currents for set A model compounds under diffusion-controlled conditions

Scan rate ($mV\,s^{-1}$)	Pt electrode		TiO_2 electrode (dark)		TiO_2 electrode (illuminated)	
	E (V)	I (μA)	E (V)	I (μA)	E (V)	I (μA)
Resorcinol (pH 6)						
25	0.87	167	1.14 ± 0.01	117 ± 8	1.14 ± 0.01	221 ± 4
50	0.87	212	1.23 ± 0.01	192 ± 9	1.26 ± 0.02	342 ± 9
100	0.93	383	1.33 ± 0.01	317 ± 22	1.33 ± 0.02	474 ± 16
150	0.96	500	1.44 ± 0.01	448 ± 11	1.45 ± 0.00	594 ± 11
200	0.97	583				
4-Chlororesorcinol (pH 6)						
25	0.78	158	1.22 ± 0.02	184 ± 8	1.27 ± 0.00	209 ± 0
50	0.83	292	1.23 ± 0.04	237 ± 13	1.31 ± 0.06	310 ± 19
100	0.88	508	1.36 ± 0.04	370 ± 8	1.35 ± 0.03	422 ± 14
150	0.90	617	1.41 ± 0.03	462 ± 21	1.41 ± 0.03	464 ± 37
200	0.95	775	1.50 ± 0.01	589 ± 23	1.42 ± 0.00	531 ± 12
4-Chlororesorcinol (pH 3)						
25	0.82	213	1.36 ± 0.00	150 ± 9	1.31 ± 0.05	209 ± 14
50	0.84	292	1.41 ± 0.01	268 ± 5	1.36 ± 0.01	288 ± 1
100	0.90	583	1.40 ± 0.01	414 ± 5	1.43 ± 0.04	355 ± 6
150	0.93	717	1.46 ± 0.03	525 ± 23	1.50 ± 0.04	511 ± 44
200	0.96	850	1.49 ± 0.04	621 ± 24	1.52 ± 0.00	619 ± 41
4,6-Dichlororesorcinol (pH 6)						
25	0.82	362	1.36 ± 0.01	233 ± 11	1.36 ± 0.00	214 ± 4
50	0.89	462	1.38 ± 0.00	322 ± 15	1.39 ± 0.00	292 ± 9
100	0.93	642	1.43 ± 0.01	483 ± 22	1.42 ± 0.00	350 ± 17
150	1.00	844	1.46 ± 0.00	577 ± 18	1.45 ± 0.20	507 ± 46
200	1.03	969	1.50 ± 0.00	614 ± 25	1.50 ± 0.20	584 ± 30

inum working electrode for comparison with the behavior on TiO_2 electrodes. The structural features of these aromatic substances with the ortho hydroxyl groups insures their chemisorption on the electrode surface to form surface chelate complexes with the titanium(IV) ions. To this extent, similar electrochemical behavior is expected among them. The resulting cyclic voltammograms, however, indicate marked differences in behavior on the platinum electrode.

Cathecol displayed a redox voltammogram (Fig. 10a) typical of a quasi-reversible system with I_{ox}/I_{red} ratio close to unity (Table 3) corresponding to a single redox reaction on the platinum working electrode. The 3,4-DHBA system displayed a similar behavior; however the I_{ox}/I_{red} ratio deviated from unity with the reduction peak approximately half that of the oxidation peak (Fig. 10b) and dependent on the scan rate (Table 3). We presume that the electrode reaction (oxidation process) was followed by a chemical reaction [45].

1,2,4-Trihydroxybenzene displayed a reversible oxidation at low oxidation potentials, ca. 0.40–0.50 V and an irre-

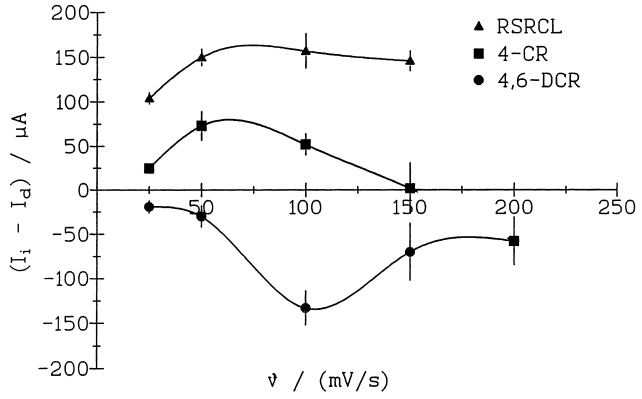

Fig. 9. Difference in peak currents on illuminated and dark particulate TiO_2 electrode as ($I_i - I_d$) vs. scan rate for the model compounds of set A.

Table 2
Redox potentials (vs. SCE) and peak currents for set A model compounds under imposed adsorption conditions

Scan rate ($mV\,s^{-1}$)	TiO_2 electrode (dark)			
	E_1 (V)	I_1 (μA)	E_2 (V)	I_2 (μA)
Resorcinol (pH 6)				
50			1.15 ± 0.01	333 ± 4
100			1.30 ± 0.01	458 ± 5
150			1.37 ± 0.01	557 ± 4
4-Chlororesorcinol (pH 6)				
50	0.63 ± 0.02	69 ± 37	1.28 ± 0.01	311 ± 10
100	0.66 ± 0.01	97 ± 13	1.27 ± 0.02	367 ± 33
150	0.65 ± 0.00	81 ± 20	1.29 ± 0.01	446 ± 31
200	0.66 ± 0.01	104 ± 13	1.41 ± 0.01	517 ± 8
4-Chlororesorcinol (pH 3)				
50	0.75 ± 0.00	133 ± 17	1.30 ± 0.00	306 ± 57
100	0.79 ± 0.01	158 ± 0	1.38 ± 0.00	400 ± 8
150	0.80 ± 0.00	158 ± 8	1.38 ± 0.02	525 ± 8
200	0.82 ± 0.00	167 ± 17	1.42 ± 0.01	443 ± 23
4,6-Dichlororesorcinol (pH 6)				
50			1.33 ± 0.02	178 ± 7
100	0.60 ± 0.01	50 ± 0	1.39 ± 0.01	261 ± 41
150	0.64 ± 0.02	58 ± 6	1.46 ± 0.01	403 ± 26
200	0.65 ± 0.01	67 ± 0	1.45 ± 0.01	450 ± 37

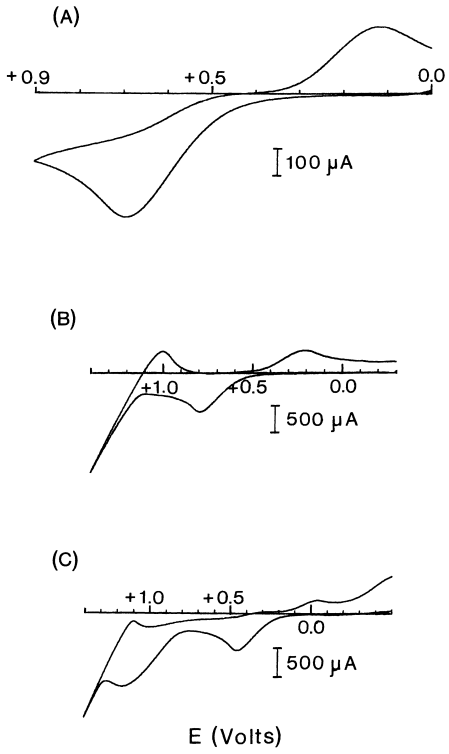

Fig. 10. Cyclic voltammograms of catechol (a), 3,4-dihydroxybenzoic acid (b), and 1,2,4-trihydroxybenzene (c) on a platinum electrode in aqueous media (see text) at a scan rate of 100 mV s^{-1}.

Table 3
Peak oxidation potentials (vs. SCE) and peak currents of set B model compounds under diffusion-controlled conditions using a platinum working electrode

Scan rate (mV s^{-1})	E_r (V)	I_r (µA)	E_1 (V)	I_1 (µA)	E_2 (V)	I_2 (µA)
Catechol (pH 6)						
25	0.21	−317	0.60	317		
50	0.16	−483	0.66	483		
100	0.11	−650	0.70	683		
150	0.10	−767	0.74	850		
200	0.08	−833	0.74	917		
Catechol (pH 3)						
25	0.21	−325	0.62	433		
50	0.16	−411	0.67	579		
100	0.12	−604	0.71	802		
150	0.10	−656	0.74	958		
200	0.08	−755	0.76	1050		
3,4-Dihydroxybenzoic acid (pH 3)						
25	0.27	−167	0.72	375		
50	0.24	−354	0.75	562		
100	0.21	−458	0.79	750		
150	0.19	−542	0.82	875		
200	0.15	−583	0.85	979		
1,2,4-Trihydroxybenzene (pH 6)						
25	0.02	−118	0.40	333	1.05	650
50	0.00	−125	0.42	584	1.10	1084
100	−0.03	−208	0.46	708	1.15	1417
150	−0.05	−250	0.47	875	1.18	1625
200	−0.08	−333	0.50	959	1.22	1875

versible oxidation at higher potentials (1.0–1.3 V; Fig. 10c) similar to those observed for quinones [40]. Peak current ratios are also different from unity (Table 3) and, in this case also, the electrode reaction was accompanied by a chemical reaction [45]. The relationship of oxidation peak currents to $\nu^{1/2}$ shows non-zero slopes and zero intercepts consistent with Eq. (1) for diffusion-controlled electrode processes (Fig. 5). Moreover, the log I–log ν linear plots (Fig. 11) provide additional support for this conclusion with slopes of ∼0.5, as expected for a diffusion-controlled oxidation process; a slope of 1 would be typical for oxidation of adsorbed species [46].

Similar experiments were carried out on TiO_2 working electrodes under otherwise identical conditions; three oxidation peaks were observed for CC (Fig. 12a) and for 3,4-DHBA) (Fig. 12b); see also Table 4. In all three cases, the oxidation peaks at the more positive potential at ca. 1.4–1.5 V (CC) and 1.3–1.4 V (3,4-DHBA) were not well resolved. Consequently, currents could not be properly measured because of this extensive overlap of oxidation peaks. Plots of peak currents versus $\nu^{1/2}$ would provide no useful information. Thus, other methods were used to probe the origin of the oxidation peaks (diffusion-controlled process or process involving adsorbed species). Multiple scans on the 3,4-DHBA system (Fig. 13) revealed that the peak currents of the two oxidation peaks at the lower potentials (∼0.7 and 0.9 V) decreased faster than the peak at the most positive potential (∼1.4 V; Table 4). We infer that the former peaks result from electrode processes involving adsorbed species that undergo a chemical reaction. The remaining oxidation peak at ∼1.4 V and the corresponding reduction peak at ca. 0.15 V correspond to a diffusion-controlled process.

Further evidence for attributing the oxidation peaks in the range of 0.60–1.10 V to adsorbed species is provided by cyclic voltammetry conducted in acetonitrile media in which adsorption was significantly diminished, if not altogether eliminated [45,46]. Cyclic voltammograms of both CC and 3,4-DHBA in this media displayed single oxidation

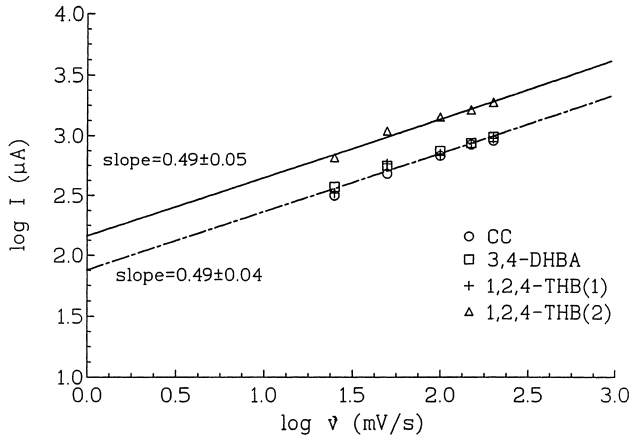

Fig. 11. Log I vs. log ν for model compounds of set B on a platinum electrode in aqueous 0.5M KCl media (see text).

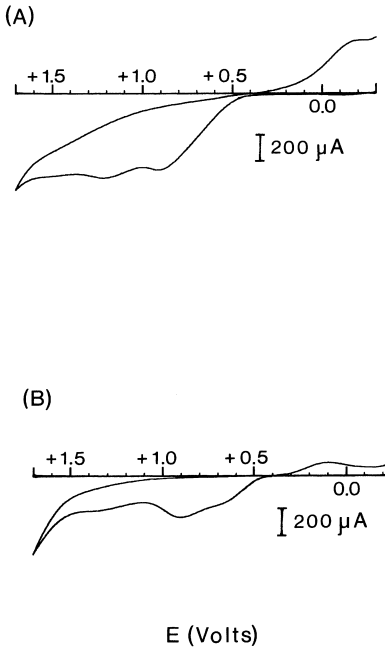

Fig. 12. Cyclic voltammograms of catechol (a) and 3,4-dihydroxybenzoic acid (b) in aqueous 0.5M KCl media on a particulate TiO_2 electrode; scan rate, $100\,mV\,s^{-1}$.

peaks at ~2.15 V and ca. 2.0 V, respectively (Figs. 14a, b). Note that the entire voltammogram is shifted toward more positive potentials in acetonitrile. The reduction peak of CC in aqueous media (at ca. −0.15 V; Fig. 12a) has shifted by 0.40 V in acetonitrile to about 0.25 V. By analogy, the oxidation peak is also expected to shift positively by a similar amount in acetonitrile. Consequently, the single oxidation peaks in acetonitrile media for CC and 3,4-DHBA are assigned to the corresponding oxidation peaks in aqueous media at the highest positive potentials (~1.4–1.5 V; Fig. 12). These observations then suggest that the additional oxidation peaks seen in aqueous media at the lower potentials of 0.9 and 1.2 V for CC and 0.7 and 0.9 V for 3,4-DHBA likely involve adsorbed CC and 3,4-DHBA species.

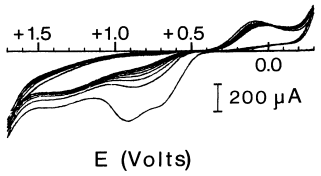

Fig. 13. Temporal behavior of the cyclic voltammogram of 3,4-dihydroxybenzoic acid in aqueous 0.5M KCl media on a particulate TiO_2 electrode and at a scan rate of $100\,mV\,s^{-1}$.

The two oxidation peaks for 1,2,4-THB were reasonably well resolved (see insert to Fig. 15). The peak current dependency on $\nu^{1/2}$ (Fig. 15) suggests that the peak at the lower oxidation potential (ca. 0.4 V) arises from an adsorbed 1,2,4-THB species, whereas the peak at the higher potential (0.7 V; Table 4) is caused by a diffusion-controlled process.

5.2. Adsorbed species

For CC, the presence of two adjacent hydroxyl groups provides a favorable structural configuration for strong

Table 4
Peak oxidation potentials (vs. SCE) and peak currents of set B model compounds under diffusion-controlled conditions using a TiO_2 working electrode (dark)

Scan rate ($mV\,s^{-1}$)	E_r (V)	I_r (μA)	E_1 (V)	I_1 (μA)	E_2 (V)	I_2 (μA)	E_3 (V)	I_3 (μA)
Catechol (pH 6)								
25	−0.06 ± 0.01	−178 ± 7	0.84 ± 0.01	342 ± 22	1.02 ± 0.02	344 ± 13		
50	−0.13 ± 0.01	−244 ± 13	0.86 ± 0.02	483 ± 33	1.01 ± 0.01	458 ± 44		
100	−0.19 ± 0.00	−329 ± 46	0.95 ± 0.02	650 ± 0.00	1.16 ± 0.03	617 ± 17		
150	−0.19 ± 0.01	−358 ± 28	0.95 ± 0.01	872 ± 52	1.19 ± 0.01	783 ± 52		
200	−0.21 ± 0.02	−428 ± 30	1.00 ± 0.02	883 ± 28	1.24 ± 0.01	817 ± 44		
Catechol (pH 3)								
25	−0.07 ± 0.00	−164 ± 13	0.82 ± 0.02	303 ± 19	1.07 ± 0.01	322 ± 20		
50	−0.12 ± 0.01	−235 ± 21	0.86 ± 0.00	411 ± 15	1.14 ± 0.01	433 ± 11		
100	−0.19 ± 0.01	−397 ± 20	0.91 ± 0.01	597 ± 15	1.22 ± 0.02	664 ± 37		
150	−0.19 ± 0.00	−401 ± 55	0.94 ± 0.02	675 ± 39	1.24 ± 0.03	703 ± 56		
200	−0.20 ± 0.00	−408 ± 6	0.97 ± 0.02	781 ± 3	1.32 ± 0.04	833 ± 56		
3,4-Dihydroxybenzoic acid (pH 3)								
25	0.11 ± 0.00	−86 ± 9	0.68 ± 0.00	267 ± 8	0.92 ± 0.00	366 ± 17	1.42 ± 0.02	264 ± 26
50	0.09 ± 0.00	−150 ± 8	0.69 ± 0.01	333 ± 8	0.92 ± 0.00	419 ± 16	1.44 ± 0.01	278 ± 14
100	0.04 ± 0.02	−279 ± 29	0.71 ± 0.01	439 ± 20	0.97 ± 0.02	600 ± 37	1.48 ± 0.02	329 ± 24
150	0.00 ± 0.00	−329 ± 60	0.71 ± 0.01	466 ± 90	0.98 ± 0.02	688 ± 35	1.50 ± 0.02	371 ± 18
200	0.01 ± 0.01	−386 ± 10	0.74 ± 0.01	532 ± 10	0.99 ± 0.01	760 ± 50	1.52 ± 0.01	364 ± 31
1,2,4-Trihydroxybenzene (pH 6)								
25			0.34 ± 0.01	334 ± 34	0.62 ± 0.01	384 ± 8		
50			0.40 ± 0.00	575 ± 42	0.69 ± 0.01	609 ± 28		
100			0.42 ± 0.02	635 ± 35	0.78 ± 0.01	802 ± 10		
150			0.45 ± 0.01	552 ± 31	0.80 ± 0.00	871 ± 36		
200			0.47 ± 0.00	625 ± 5	0.87 ± 0.03	1040 ± 41		

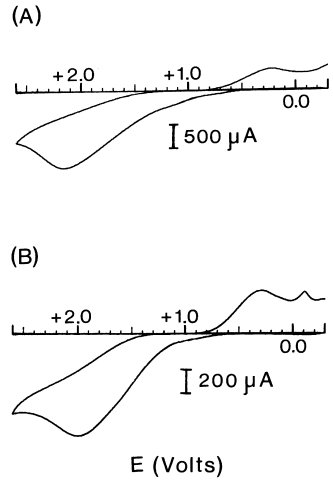

Fig. 14. Cyclic voltammograms of catechol (a) and 3,4-dihydroxybenzoic acid (b) in acetonitrile media on a particulate TiO_2 electrode (see text) at a scan rate of $100\,mV\,s^{-1}$.

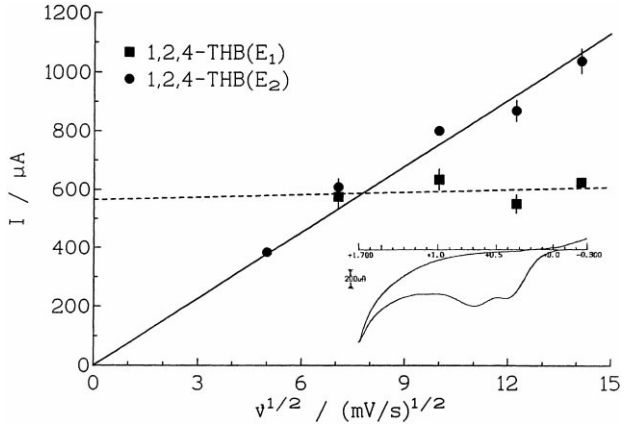

Fig. 15. Oxidation peak current, I_p, vs. the square root of the scan rate for 1,2,4-trihydroxybenzene in aqueous media on the particulate TiO_2 electrode (see text). Insert shows the voltammogram for 1,2,4-THB in aqueous media at a scan rate of $50\,mV\,s^{-1}$.

adsorption on the TiO_2 surface [32,33]. Since CC is very polar due to these ortho OH substituents, all the material deposited on the electrode surface is expected to be adsorbed. By contrast, 3,4-DHBA and 1,2,4-THB contain an additional functional group on the ring carbon 4, which diminishes the polarity relative to CC. Thus, for the same amount of material placed on the electrode surface, less adsorption should take place allowing a fraction of 3,4-DHBA and 1,2,4-THB to diffuse into the solution and show up as an additional oxidation peak (diffusion-controlled). Two peaks were readily seen for 3,4-DHBA and 1,2,4-THB (Table 5).

Under imposed adsorption conditions, the peak at ca. 0.5–0.7 V in the solubilized 3,4-DHBA was barely noticeable at ~0.7 V (Fig. 16; Table 5), in contrast to the three oxidation peaks easily observed for solubilized 3,4-DHBA (see Fig. 12b). The peaks at ca. 0.7 and 0.9–1.0 V are due to adsorption of 3,4-DHBA via the two functionalities, namely the ortho OH groups and the $–COO^-$ group at the 4-position. For 1,2,4-THB, adsorption can take place through the ortho OH groups (strong), and through the OH group at the 4-position, if at all (weak).

5.3. Effect of illumination

The photoelectrochemical behavior of CC, 3,4-DHBA and 1,2,4-THB compounds was also examined on illuminated TiO_2 electrodes to compare with the behavior observed in the dark. Only slight changes in peak currents were detected for these compounds under illumination (Table 6).

Table 5
Oxidation peak potentials (vs. SCE) and peak currents for set B model compounds under imposed adsorption conditions using a TiO_2 working electrode (dark)

Scan rate ($mV\,s^{-1}$)	E_o (V)	I_o (μA)	E_1 (V)	I_1 (μA)	E_2 (V)	I_2 (μA)
Catechol (pH 6)						
50	0.84 ± 0.00	378 ± 20				
100	0.90 ± 0.03	447 ± 10				
150	0.91 ± 0.01	569 ± 34				
200	0.95 ± 0.01	618 ± 27				
Catechol (pH 3)						
50	0.84 ± 0.01	314 ± 20				
100	0.87 ± 0.01	383 ± 33				
150	0.89 ± 0.01	443 ± 37				
200	0.91 ± 0.01	556 ± 13				
3,4-Dihydroxybenzoic acid (pH 3)						
50			0.96 ± 0.01	365 ± 9	1.46 ± 0.03	249 ± 49
100			1.02 ± 0.01	479 ± 73	1.53 ± 0.15	305 ± 49
150			1.08 ± 0.00	646 ± 50	1.57 ± 0.07	344 ± 7
200			1.06 ± 0.02	625 ± 55	1.55 ± 0.04	354 ± 14
1,2,4-Trihydroxybenzene (pH 6)						
50			0.43 ± 0.02	467 ± 25	0.70 ± 0.02	533 ± 22
100			0.55 ± 0.03	1040 ± 31	0.80 ± 0.04	1104 ± 18
150			0.68 ± 0.01	1021 ± 15	0.95 ± 0.02	1229 ± 28
200			0.67 ± 0.02	1042 ± 45	0.98 ± 0.03	1375 ± 39

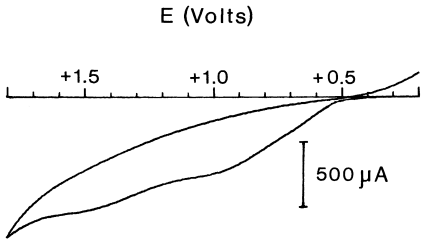

Fig. 16. Cyclic voltammogram of 3,4-dihydroxybenzoic acid in aqueous media on a particulate TiO_2 electrode under imposed adsorption conditions (see text).

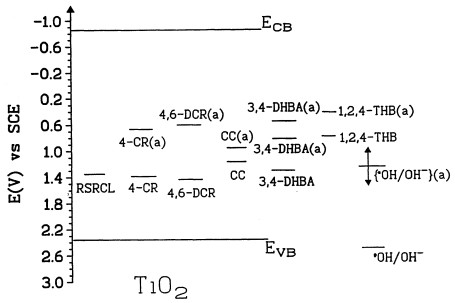

Fig. 17. Redox potentials plot showing the potentials (vs. SCE) of the conduction and valence bands of TiO_2 at pH 6 and the oxidation potentials of the free and adsorbed (a) model compounds examined in aqueous media at a scan rate of $100\,mV\,s^{-1}$. Also shown are the relevant potentials for the $^{\bullet}OH/OH^{-}$ couple in homogeneous aqueous phase (vs. SCE) and as an adsorbed $^{\bullet}OH(a)$ radical on TiO_2 double-headed arrow is the uncertainty of this redox potential; see [47].

Catechol and 3,4-dihydroxybenzoic acid each showed a reduction peak in the dark. For CC, the reduction peak vanished under illumination and the one for 3,4-DHBA was reduced to about half of its dark value. The absence of the reduction peak for CC and the smaller reduction current for 3,4-DHBA are likely due to the band structure of TiO_2 which does not favor a reduction process under illumination and under the present circumstances. When irradiated, the surface of the TiO_2 electrode is positively charged due to migration of holes to the surface (electrons move in opposite direction toward the external circuit); hence, removal of an electron from the electrode surface to cause reduction of an adsorbed substrate becomes highly unfavorable. Illumination of the electrode also leads to a shift in the baseline of the voltammogram (see Fig. 8) indicating photoactivity of the TiO_2. The magnitude of the baseline shift, maximum for CC and decreasing to zero for 1,2,4-THB, depends on the type of organic substance in solution and on its polarity, as estimated using the PC MODELLING software: CC > 3,4-DHBA > 1,2,4-THB.

5.4. Effect of pH

The redox behavior of CC was first examined on a platinum working electrode at pH 3 and 6 (Table 3), and then compared to results obtained on TiO_2 electrodes in the dark (Table 4). Oxidation potentials of CC remained invariant at these pHs on the Pt electrode; however, oxidation peak currents were slightly greater at pH 3, whereas reduction peak currents were lower at pH 3 compared to

Table 6
Peak oxidation potentials (vs. SCE) and peak currents of set B model compounds under diffusion-controlled conditions using a TiO_2 working electrode (illuminated)

Scan rate ($mV\,s^{-1}$)	E_r (V)	Ir (μA)	E_1 (V)	I_1 (μA)	E_2 (V)	I_2 (μA)	E_3 (V)	I_3 (μA)
Catechol (pH 6)								
25			0.80 ± 0.01	233 ± 25	0.97 ± 0.01	188 ± 13		
50			0.88 ± 0.00	406 ± 15	1.07 ± 0.01	396 ± 12		
100			0.95 ± 0.01	544 ± 44	1.19 ± 0.02	539 ± 44		
150			0.99 ± 0.01	750 ± 42	1.25 ± 0.03	636 ± 11		
200			1.06 ± 0.02	883 ± 50	1.28 ± 0.00	750 ± 21		
Catechol (pH 3)								
25			0.84 ± 0.01	292 ± 25	1.00 ± 0.03	275 ± 25		
50			0.87 ± 0.00	333 ± 0	1.15 ± 0.00	342 ± 8		
100			0.94 ± 0.01	453 ± 16	1.24 ± 0.02	474 ± 26		
150			0.96 ± 0.01	545 ± 57	1.28 ± 0.02	639 ± 46		
200			1.00 ± 0.02	615 ± 49	1.39 ± 0.00	778 ± 60		
3,4-Dihydroxybenzoic acid (pH 3)								
25			0.68 ± 0.01	257 ± 17	0.91 ± 0.01	377 ± 27	1.49 ± 0.01	233 ± 20
50			0.69 ± 0.01	344 ± 22	0.95 ± 0.00	522 ± 19	1.49 ± 0.01	328 ± 14
100	0.09 ± 0.01	−125 ± 21	0.72 ± 0.02	417 ± 47	0.97 ± 0.02	572 ± 38	1.51 ± 0.02	354 ± 11
150	0.01 ± 0.01	−229 ± 11	0.71 ± 0.01	549 ± 7	1.01 ± 0.00	757 ± 28	1.52 ± 0.01	354 ± 13
200	0.00 ± 0.01	−287 ± 19	0.72 ± 0.01	617 ± 18	1.04 ± 0.00	861 ± 41	1.57 ± 0.01	382 ± 21
1,2,4-Trihydroxybenzene (pH 6)								
25			0.43 ± 0.02	550 ± 33	0.67 ± 0.02	475 ± 58		
50			0.48 ± 0.03	675 ± 25	0.80 ± 0.03	659 ± 9		
100			0.49 ± 0.01	756 ± 6	0.78 ± 0.01	833 ± 21		
150			0.52 ± 0.01	896 ± 42	0.86 ± 0.03	938 ± 40		
200			0.57 ± 0.01	729 ± 5	0.99 ± 0.02	1070 ± 70		

pH 6. These observations are consistent with CC undergoing some self-oxidation at the higher pH [44].

Oxidation potentials of species adsorbed on TiO_2 remained the same regardless of pH at which the experiments were carried out (ca. 0.8–1.0 V; E_1 in Table 4). However, oxidation at the most positive potentials (diffusion-controlled process) varied slightly with change in pH, shifting to more negative potentials at pH 6. It appears that only oxidation potentials of diffusion-controlled processes then may be affected by changes in the band positions of TiO_2 associated with the pH changes (band positions change by ca. $-0.06 \times \Delta$pH) .

6. Conclusions

Results obtained in this study show that the (photo)electrochemical behavior of the aromatic substances examined depend on the type and nature of the working electrode used and on the polar characteristics of these substances. Weakly adsorbed species display similar redox behaviors on both Pt and TiO_2 electrodes. Separate oxidation peak potentials were seen for adsorbed and free species, with the differences in the range ~0.2–0.8 V. The reversibility of the redox process of strongly adsorbed organics (set B) diminishes on TiO_2 due to the band structure and the nature of the electrode surface; in the present instance, reduction is unfavorable. Multiple oxidation peak potentials were detected on the TiO_2 electrodes for strongly adsorbed systems. The peak at the most positive potentials has been ascribed to diffusion-controlled processes, whereas those at more negative potentials have been attributed to processes arising from adsorption. Based on these findings, predictions and quantitative estimates of the driving force for photooxidations in heterogeneous photocatalysis based on flat band potentials of the semiconductor photocatalyst (here TiO_2) and on the Fermi levels of the redox couples in solution (Fig. 17) need to be revisited.

Acknowledgements

We are grateful to the Natural Sciences and Engineering Research Council of Canada for support of our work (ML and NS).

References

[1] P.H. Abelson, Science 224 (1984) 673.
[2] J. Long, Chem. Eng. News 62 (1984) 20.
[3] D.F. Ollis, in: M. Schiavello (Ed.), Photocatalysis and the Environment, Kluwer Academic Publishers, Dordrecht, 1989, pp. 663–677.
[4] C.S. Turchi, D.F. Ollis, J. Catal. 122 (1990) 178.
[5] A.L. Linsebigler, G. Lu, J.T. Yates, Chem. Rev. 95 (1995) 735.
[6] H. Al-Ekabi, N. Serpone, J. Phys. Chem. 92 (1988) 5726.
[7] K. Vinodgopal, U. Stafford, K.A. Gray, P.V. Kamat, J. Phys. Chem. 98 (1994) 6797.
[8] K. Vinodgopal, S. Hotchandani, P.V. Kamat, J. Phys. Chem. 97 (1993) 9040.
[9] H. Gerischer, A. Heller, J. Electrochem. Soc. 139 (1992) 113.
[10] U. Stafford, K.A. Gray, P.V. Kamat, A. Varma, Chem. Phys. Lett. 55 (1993) 205.
[11] R.W. Matthews, J. Phys. Chem. 91 (1987) 3328.
[12] J. Sabate, M.A. Anderson, H. Kikkawa, M. Edwards, C.G. Hill, J. Catal. 127 (1991) 167.
[13] M.W. Peterson, J.A. Turner, A.J. Nozik, J. Phys. Chem. 95 (1991) 221.
[14] J.-M. Herrmann, P. Pichat, J. Chem. Soc. Faraday Trans. 1 76 (1980) 1138.
[15] R.W. Matthews, J. Catal. 111 (1988) 264.
[16] M. Barbeni, E. Pramauro, E. Pelizzetti, E. Borgarello, M. Gratzel, N. Serpone, Nouv. J. Chim. 8 (1984) 547.
[17] M. Barbeni, E. Pramauro, E. Pelizzetti, M. Vincenti, E. Borgarello, M. Gratzel, N. Serpone, M.A. Jamieson, Chemosphere 15 (1986) 1913.
[18] R. Terzian, N. Serpone, C. Minero, E. Pelizzetti, J. Catal. 128 (1991) 352.
[19] A. Mills, S. Morris, R. Davies, J. Photochem. Photobiol. A: Chem. 70 (1993) 183.
[20] A. Mills, S. Morris, J. Photochem. Photobiol. A: Chem. 71 (1993) 285.
[21] T. Sehili, P. Boule, J. Lemaire, J. Photochem. Photobiol. A: Chem. 50 (1989) 117.
[22] K. Okamoto, Y. Yamamoto, H. Tanaka, M. Tanaka, A. Itaya, Bull. Chem. Soc. Jpn. 58 (1985) 2015.
[23] V. Augugliaro, L. Palmisano, A. Sclafani, C. Minero, E. Pelizzetti, Toxicol. Environ. Chem. 16 (1988) 89.
[24] T. Nguyen, D.F. Ollis, J. Phys. Chem. 88 (1984) 3386.
[25] B. Kreutler, A.J. Bard, J. Am. Chem. Soc. 100 (1978) 2339.
[26] H.O. Finklea, J. Chem. Ed. 60 (1983) 325.
[27] N. Serpone, E. Pelizzetti, Photocatalysis-Fundamentals and Applications, Wiley, New York, 1989.
[28] M.A. Fox, M.T. Dulay, Chem. Rev. 93 (1993) 341.
[29] J. Moser, S. Punchihewa, P.P. Infelta, M. Gratzel, Langmuir 7 (1991) 3012.
[30] A.T. Hubbard, F.C. Anson, J. Anal. Chem. 38 (1996) 58.
[31] R.H. Wopschall, I. Shain, J. Anal. Chem. 39 (1967) 1514.
[32] S. Tunesi, M.A. Anderson, J. Phys. Chem. 95 (1991) 3399.
[33] S. Tunesi, M.A. Anderson, Langmuir 8 (1992) 489.
[34] J. McMurry, Organic Chemistry, 2nd ed., Brooks-Cole Publ., Pacific Grove, CA, 1988.
[35] A.L. Terney, Comparative Organic Chemistry, Saunders, Toronto, 1976.
[36] W. Schmikler, Interfacial Electrochemistry, Oxford University Press, Oxford, 1996.
[37] C.A. Koval, J.N. Howard, Chem. Rev. 92 (1992) 411.
[38] C. Sinn, D. Meissner, R. Memming, J. Electrochem. Soc. 137 (1990) 168.
[39] M. Etman, J. Phys. Chem. 90 (1986) 1844.
[40] D.T. Sawyer, A. Sobkowiak, J.L. Roberts, Electrochemistry for Chemists, 2nd ed., Wiley, New York, 1995.
[41] S.G. Yan, J.T. Hupp, J. Phys. Chem. 100 (1996) 6867.
[42] G. Redmond, D. Fitzmaurice, J. Phys. Chem. 97 (1993) 1426.
[43] H.O. Finklea, Semiconductor Electrodes, Elsevier, New York, 1988, p. 80
[44] N. Serpone, G. Sauve, R. Koch, H. Tahiri, P. Pichat, P. Piccinini, E. Pelizzetti, H. Hidaka, J. Photochem. Photobiol. A: Chem. 84 (1996) 191.
[45] D.K. Grosser Jr., Cyclic Voltammetry Simulation and Analysis of Reaction Mechanisms, VCH Publisher, New York, 1993.
[46] P.T. Kissinger, W.R. Heineman, Laboratory Techniques in Electroanalytical Chemistry, Marcel Dekker, New York, 1984.
[47] D. Lawless, N. Serpone, D. Meisel, J. Phys. Chem. 95 (1991) 5166.